Monatomic Chemical-Vapor-Deposited Graphene Membranes Bridge a Half-Millimeter-Scale Gap

Choong-Kwang Lee,[†,‡,∥] Yun Hwangbo,[†,∥] Sang-Min Kim,[†] Seoung-Ki Lee,[§] Seung-Mo Lee,[†] Seong-Su Kim,[‡] Kwang-Seop Kim,[†] Hak-Joo Lee,[†] Byung-Ik Choi,[†] Chang-Kyu Song,[⊥] Jong-Hyun Ahn,[§,*] and Jae-Hyun Kim[†,*]

[†]Department of Nano-Mechanics, Korea Institute of Machinery & Materials (KIMM), 156 Gajungbuk-ro, Yuseong-gu, Daejeon 305-343, South Korea, [‡]Department of Organic Materials & Fiber Engineering, Chonbuk National University, Jeonju 561-756, South Korea, [§]School of Electrical and Electronic Engineering, Yonsei University, Seoul 120-749, South Korea, and [⊥]Department of Ultra-Precision System, Korea Institute of Machinery & Materials (KIMM), 156 Gajungbuk-ro, Yuseong-gu, Daejeon 305-343, South Korea. [∥]These authors contributed equally to this work.

ABSTRACT One of the main concerns in nanotechnology is the utilization of nanomaterials in macroscopic applications without losing their extreme properties. In an effort to bridge the gap between the nano- and macroscales, we propose a clever fabrication method, the inverted floating method (IFM), for preparing freestanding chemical-vapor-deposited (CVD) graphene membranes. These freestanding membranes were then successfully suspended over a gap a half-millimeter in diameter. To understand the working principle of IFM, high-speed photography and white light interferometry were used to characterize and analyze the deformation behaviors of the freestanding graphene membranes in contact with a liquid during fabrication. Some nanoscale configurations in the macroscopic graphene membranes were able to be characterized by simple optical microscopy. The proposed IFM is a powerful approach to investigating the macroscopic structures of CVD graphene and enables the exploitation of freestanding CVD graphene for device applications.

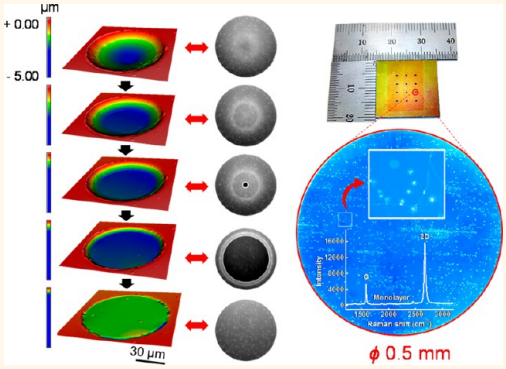

KEYWORDS: CVD graphene · freestanding membrane · rupture · microscopy · mechanics

Scale bridging presents an obstacle to the engineering of nanotechnology applications. Utility in daily life requires that nanomaterials be incorporated into macroscale applications without disturbing their extraordinary properties. Current manufacturing techniques are generally unable to fully overcome the size differences between the nano- and macroscales. Nanomaterials lose their unique properties when they coalesce into larger structures or make contact with bulk substrates. For example, the two-dimensional nanomaterial, graphene, often loses its highest charge carrier mobility when it contacts a bulk substrate.[1,2] Nanowires and quantum dots tend to aggregate if special precautions are not taken during fabrication to prevent coalescence. The aggregates do not normally display the same nanoscale properties. It is critical to develop methods through which nanomaterials may bridge multiple length scales to enable their use in macroscale applications.

Graphene displays excellent physical properties; however, it suffers from the scale-bridging issue in pressure sensor,[3,4] gas detector,[5−7] acoustic metamaterial,[8] and resonator[9−11] applications. These applications would benefit from the fabrication of monatomic freestanding graphene membranes with large lateral dimensions. Some research groups have reported techniques for fabricating suspended or freestanding graphene on a perforated substrate based on patterning and electroplating,[12] patterning and direct etching of a metal catalyst,[13] or wet transfer making use of a polymeric film as a supporting layer during the etching process of a metal catalyst.[14] The wet transfer method prevails nowadays due to its scalability and compatibility to a silicon micromachining process. Freestanding graphene membranes are frequently ruptured

* Address correspondence to jaehkim@kimm.re.kr, ahnj@yonsei.ac.kr.

Received for review November 8, 2013 and accepted February 25, 2014.

Published online February 25, 2014
10.1021/nn405805s

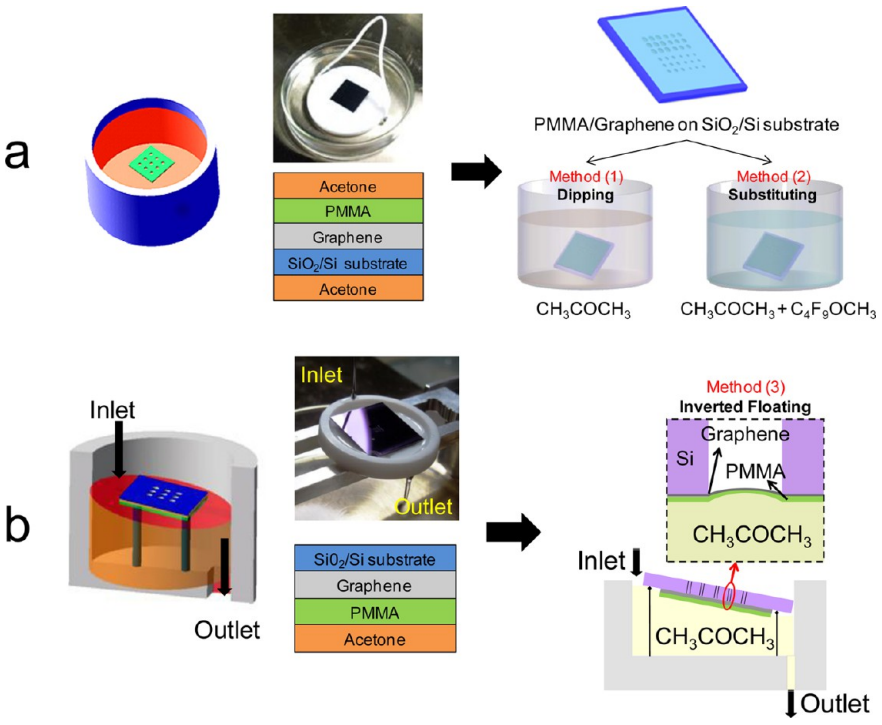

Figure 1. Conventional and novel PMMA removal methods for fabricating freestanding CVD graphene. (a) Conventional dipping methods. In methods 1 and 2, acetone (CH_3COCH_3) is used as an etchant to remove PMMA. In method 2, acetone is gradually substituted with methoxynonafluorobutane ($C_4F_9OCH_3$) after etching away the PMMA. (b) Inverted floating method, method 3, is schematically illustrated. In this method, acetone only contacts the PMMA, which prevents the intrusion of the etchant into the through-holes.

during etching of the supporting layer and subsequent drying of the liquid etchant. The size and yield are consequently limited by the delicacy of the membranes. The reported size of a freestanding graphene membrane prepared on a perforated substrate is typically on the order of tens of micrometers in most cases.[15−17]

Here, we present an effective method for fabricating freestanding chemical-vapor-deposited (CVD) graphene membranes that can bridge gaps up to a half-millimeter scale without losing the monatomic nature of the membrane. The working principle underlying the proposed method is described based on an understanding of the interaction between the graphene membrane and a liquid. This interaction was visualized using high-speed optical photography and white light interferometry (WLI) techniques. The large freestanding membrane permitted the macroscopic inspection of CVD graphene. Some nanoscale configurations including wrinkles, cracks, pinholes, and multilayer islands on the CVD graphene were readily identified using simple optical microscopy techniques. The proposed method is a powerful route to examine the quality of synthesized graphene and enables the exploitation of freestanding CVD graphene with large scale and high yield for device applications.

RESULTS AND DISCUSSION

Fabrication of Large Freestanding CVD Graphene Membranes. The graphene used in this study was grown by CVD methods as described previously.[18] Freestanding CVD graphene was fabricated using typical procedures, including graphene growth, polymethyl methacrylate (PMMA) spin-coating, copper foil etching, rinsing, and wet transfer onto a perforated SiO_2 substrate (Supporting Information Figure S1). These are conventional procedures for transferring CVD graphene onto a variety of substrates.[19−21] CVD graphene protected by a PMMA layer may be readily transferred onto a perforated substrate with negligible damage. To obtain freestanding CVD graphene, however, the PMMA layer used in the fabrication procedures must be carefully removed. The process for removing the PMMA layer using a chemical etchant and drying the etchant is the most important step because most of the freestanding graphene membranes are ruptured during this step.

Figure 1 shows three different methods for removing PMMA to produce freestanding CVD graphene. Acetone was used as a solvent to dissolve PMMA. Method 1 is the conventional dipping process in which the whole sample is submerged into acetone. Method 2 is a substitution method in which acetone is gradually substituted with methoxynonafluorobutane ($C_4F_9OCH_3$), which has a low surface tension, after removing the PMMA with acetone. Since $C_4F_9OCH_3$ cannot dissolve the PMMA layer, it was just utilized for reducing the surface tension of acetone. Method 3 is described here for the first time. In method 3, the sample is floated on the surface of an acetone bath without introducing a

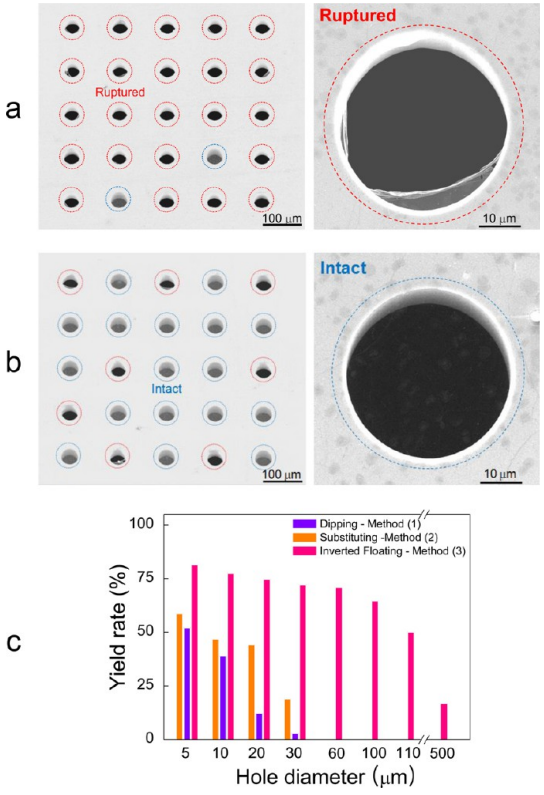

Figure 2. SEM images of the freestanding graphene and the yield rates for the various PMMA etching methods. Intact freestanding CVD graphene membranes are marked by blue circles, and ruptured membranes are marked by red circles. (a) Conventional dipping method provided a low yield, whereas (b) the majority of holes were covered by intact CVD graphene membranes after using the IFM. (c) Statistical results of the yield rates for the three methods showed that freestanding CVD graphene membranes could be fabricated with diameters up to 500 μm using IFM. The difference between the yield rates of methods 1 and 2 suggested that the surface tension of the liquid was closely related to the rupture of the freestanding CVD graphene.

liquid into the holes underneath the graphene membrane. The whole sample is not submerged in acetone, and only the PMMA layer makes contact with acetone. This technique, hereafter, will be called the inverted floating method (IFM). In IFM method, the PMMA was removed by acetone flowing across it. To completely remove the PMMA, the sample was tilted at a very small angle and dissolution was performed for over several hours. The conventional method 1 often results in ruptures in most of graphene membranes, but method 2 provides somewhat better yields, suggesting that the ruptures are related to the surface tension of the liquid in contact with the membrane.[14,22] The surface tensions of the liquids utilized in this report are listed in the Supporting Information Table S1.[23]

Figure 2a,b shows the typical SEM images of the membranes obtained using method 1 and method 3, respectively. Intact CVD graphene membranes covering the holes are indicated by blue circles, and ruptured ones are indicated by red circles. Most of the holes remained covered by intact freestanding CVD graphene when prepared using method 3, whereas the conventional method 1 led to poor coverage.

Figure 2c shows the yield rates of the three methods. The yield rates for the various membrane diameters are listed in the Supporting Information Table S2. Here, the yield rate is defined as the ratio of the number of intact freestanding graphene membranes present before and after the etching and drying processes. The yield rates for methods 1 and 2 were less than 60%, even for the small holes (5 μm). These yield rates decreased dramatically as the hole size increased, and they approached 0% for holes larger than 30 μm in diameter. A comparison of methods 1 and 2 shows that the yield rate of method 2 was higher than that of method 1, especially for the larger holes (20 and 30 μm). On the other hand, method 3 displayed superior yield rates regardless of the hole size and allowed for the successful fabrication of very large freestanding graphene up to 0.5 mm, while methods 1 and 2 did not consistently provide freestanding CVD graphene membranes larger than 60 μm in diameter. The membranes from 0.1 to 0.5 mm in diameter were not tried due to the absence of the silicon substrates having those hole sizes. Regarding the yield rates obtained in this report, it is worthy to note that the yield rate might be affected by not only the process of PMMA removal but also several other factors such as quality of CVD graphene, etching of copper foil, and handling of graphene during transfer. All these factors were carefully practiced in a batch manner to reveal only the effect of the process for PMMA removal. In addition, compared with the critical point drying (CPD) method, IFM method has advantage over CPD in creation of a large area freestanding graphene membrane because the complicated flow of liquid CO_2 and solvents as well as the high pressure and low temperature inside a CPD chamber can easily cause the rupture of graphene membranes.

Rupture Mechanism and the Working Principle of the IFM Technique. The difference in the yield rates among the three methods and the working principle underlying the IFM were systematically investigated by characterizing the mechanics of the drying process and the rupture mechanism. After removing the PMMA layer from the graphene membranes using acetone, the samples were removed from the acetone and were gradually dried under atmospheric conditions. Acetone on the top surface of the freestanding graphene evaporated faster than acetone inside the hole beneath the freestanding graphene due to the tiny volume of the hole in the perforated substrate. The acetone remaining inside the hole exerted a mechanical load on the graphene. Figure 3 shows high-speed camera images and the corresponding schematic diagrams of the sequential changes during the deformation of the freestanding CVD graphene loaded by the surface tension as the liquid dries out (see the Supporting Information movie S1). The freestanding graphene

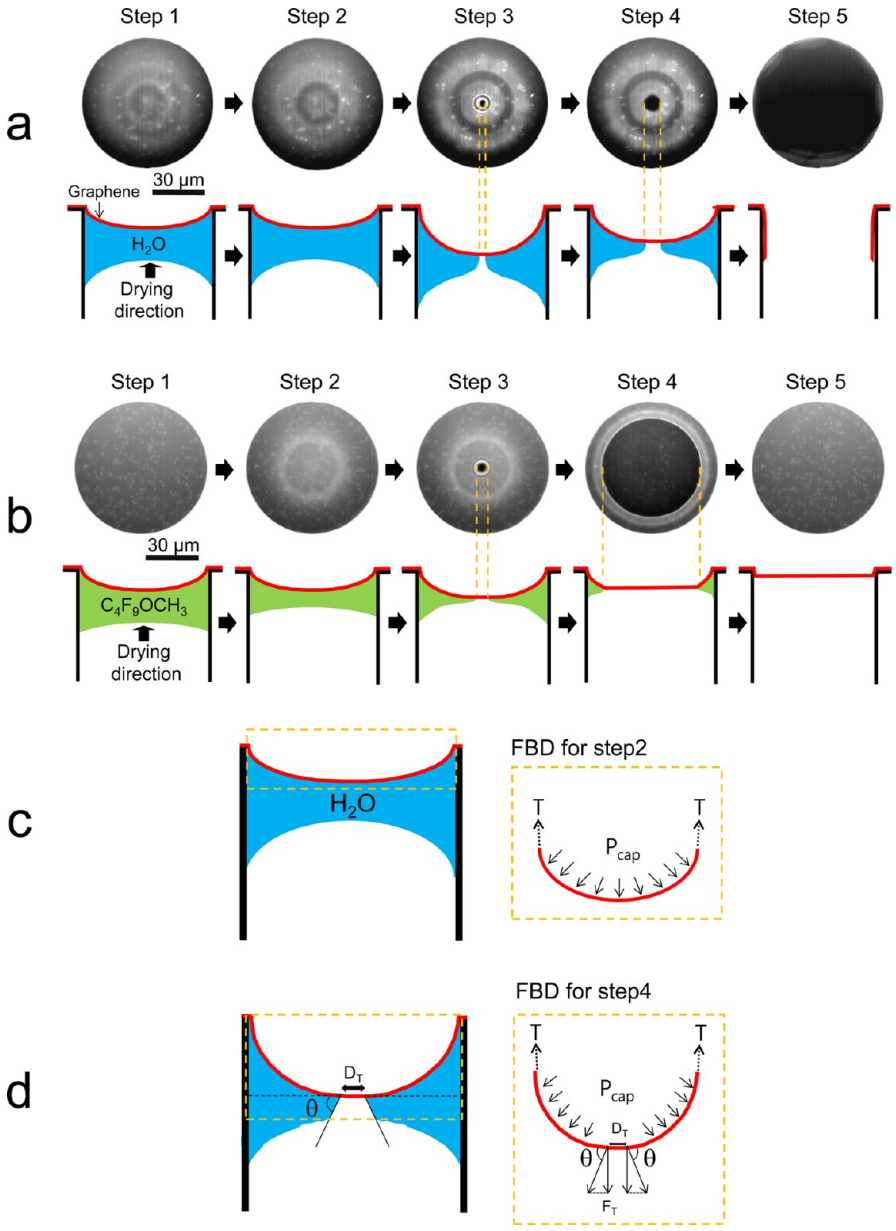

Figure 3. High-speed camera images, corresponding schematic illustrations, and free-body diagrams of the freestanding graphene membranes loaded by the surface tension of a liquid during the drying process. The high-speed camera images and the corresponding schematic illustrations show the sequential changes experienced by the deformed graphene membranes during the drying process in (a) a case in which the membrane ruptured and (b) a case in which the membrane remained intact after the liquid had completely dried. (c) Freestanding membrane in step 2 of panel (a) experienced the capillary pressure induced by the liquid entrapped in the hole, and (d) freestanding membrane in step 4 of panel (a) experienced both the capillary pressure and the triple junction force due to the formation of a triple junction arc on the bottom face of the graphene.

deformed downward due to the loading and was ruptured, depending on the magnitude of the load and the defect distribution over the graphene membrane.

The load induced by the surface tension was evaluated by modeling the hole as a capillary containing a liquid drop. The pressure induced in a capillary is given as follows.[24]

$$P_{cap} = \frac{4\lambda \cos\phi}{D} \quad (1)$$

where P_{cap} is the capillary pressure, λ is the surface tension of the liquid, ϕ is the contact angle between the capillary wall and the liquid, and D is the diameter of the capillary. This equation is valid only when the bottom face of the freestanding graphene is completely covered with the liquid. The free-body diagram (FBD) for this system is shown in Figure 3c. The contact angles of the liquids used in the experiments are shown in Figure S2. As the liquid inside the capillary dried, the center portion of the bottom face of the freestanding graphene became exposed to air, and eq 1 was no longer valid. At this moment, the liquid suddenly moved outward and downward due to the formation of a triple junction arc consisting of the graphene, liquid,

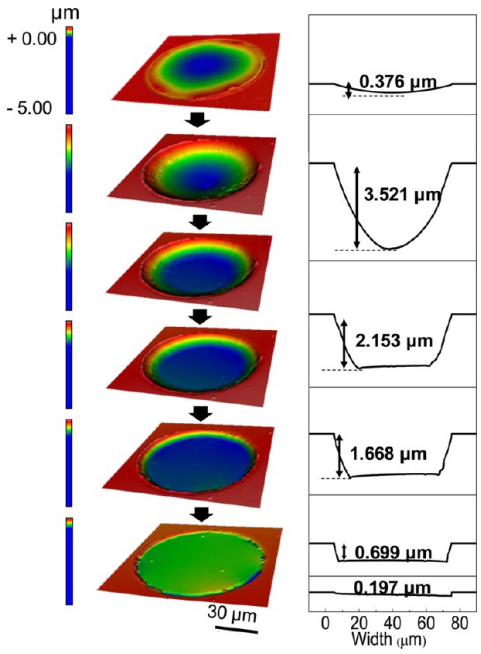

Figure 4. Sequential WLI measurements during the deformation of a freestanding CVD graphene membrane during the water drying process. The bulge shape of the freestanding graphene membrane with a diameter of 70 μm was measured using WLI. As the water dried, the central region of the membrane stretched, and the stretched region increased continuously until the end of the drying process.

and air, as shown in step 3 (Figure 3a,b). The configurational change in the liquid introduced an additional force on the freestanding membrane and led to a large downward deformation. When the diameter of the triple junction arc is small, the induced force can be modeled as a concentrated load at the center of the freestanding graphene, and its magnitude is several micronewtons. The corresponding FBD is shown in Figure 3d. The corresponding deflection by the triple junction can be on the order of micrometers. The large deformation of the freestanding graphene is discussed in detail in the Supporting Information Figure S3. Figure 3a shows a graphene membrane that failed to survive during the drying process, whereas Figure 3b shows a graphene membrane that survived after the liquid had been completely removed by drying. The central region of a freestanding graphene membrane having negligible defects and subjected to a liquid with a small surface tension will become exposed to air. Otherwise, the graphene membrane could fail even before or right after exposure. This central region, then, grows toward the boundary of the capillary, as shown in Figure 3b. Once the liquid has completely dried, the graphene membrane will remain suspended on the capillary and will experience some residual stress.

The deformation of the freestanding CVD graphene during the liquid drying process was investigated by precisely measuring the shape of the deformed graphene with white light interferometry (WLI), as shown in Figure 4. Distilled water was used as the test liquid in

TABLE 1. Summary of the Maximum Stress and Strain on the Freestanding CVD Graphene Samples

diameter (μm)	deflection$_{max}$ (μm)	strain$_{max}$ (%)	stress$_{max}$ (GPa)	$P_{capillary}$ (kPa)	liquid
40	1.70	0.495	5.90 ± 1.50	2.31	CH_3COCH_3
50	1.99	0.450	5.39 ± 1.37	1.85	CH_3COCH_3
60	2.46	0.477	5.70 ± 1.45	1.54	CH_3COCH_3
70	3.52	0.673	7.94 ± 2.02	3.92	H_2O
100	3.87	0.451	5.40 ± 1.37	0.922	CH_3COCH_3

this measurement. From the measured profile obtained by WLI, the induced strain ε_r in the freestanding graphene could be estimated from the total length of the deformed graphene, and the corresponding stress in the graphene could be estimated according to the following equation:

$$\sigma_r = \frac{E}{1-\nu}\varepsilon_r + \sigma_0 \quad (2)$$

where σ_0 represents the residual stress and E and ν are the elastic modulus and Poisson's ratio, respectively. The residual stress in the freestanding graphene was assumed to remain constant during the drying process, with a typical value of about 250 MPa for the freestanding CVD graphene,[17] and Poisson's ratio of the CVD graphene was assumed to be 0.165.[25,26] The elastic modulus (E = 955 ± 243 GPa) for CVD graphene was statistically estimated on the basis of previous reports[26,27] because it may vary from sample to sample (Figure S4). The strain and corresponding stress at the maximum deflection could then be calculated for several freestanding graphene samples as in Table 1. In many of our experiments, the graphene membranes were observed to rupture predominantly under the maximum deflection conditions.

The maximum stress shown in Table 1 varied from 5.39 to 7.94 GPa. This maximum stress was much lower than the theoretical strength that was calculated using density functional theory with consideration of the grain boundary structures in CVD graphene[28] and recently obtained experimental result of the small-sized CVD graphene membrane.[26] The low rupture strength of large-sized CVD graphene in this study might be attributed to the many overlapped grain boundaries and the microscopic flaws which could be generated by various graphene growth conditions. The bonding forces between adjacent grains in the overlapping regions were not covalent; rather, they were physical van der Waals bonds.[26,29] It was recently found that these regions could significantly reduce the apparent strength of the CVD graphene.[26] In addition, we frequently observed microscopic defects, such as circular or elliptical pinholes, in the vicinity of multilayer islands and wrinkles in our freestanding CVD graphene, as shown in Figure S5. These microscopic defects can further reduce the apparent strength of graphene and nucleate ruptures

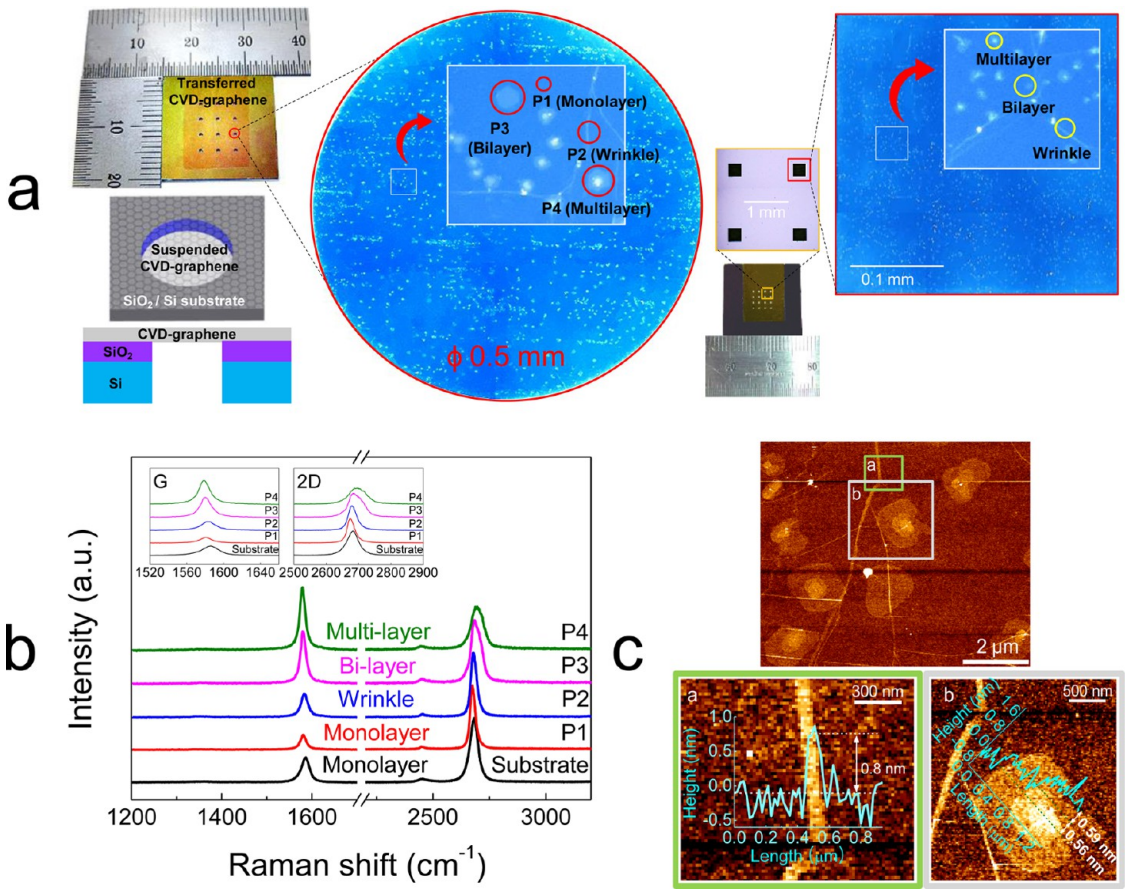

Figure 5. Characterization of the freestanding CVD graphene with a large dimension. (a) Optical microscopy images of the freestanding CVD graphene membranes across a circular hole 0.5 mm in diameter and a square hole 0.3 mm in length on perforated Si/SiO_2 substrates. (b) Raman spectra measured at various positions on the freestanding graphene membrane. (c) AFM images obtained by scanning over a wrinkle and a multilayer island.

during the drying process, even under stresses much lower than the theoretical strength of the polycrystalline graphene, as discussed in the text associated with Figure S5. The microscopic defects could explain the decrease in the yield rate, shown in Figure 2c, with the increase in the size of the graphene because the number of defects increased in proportion to the area of the freestanding region.

The rupture mechanism of freestanding graphene depended on the presence of liquid entrapped in the capillary-like perforated substrate hole during the drying process after etching away the PMMA support. The yield rate may be significantly increased by preventing the liquid from intruding into the capillary, as in the IFM. Figure 1b shows that the PMMA layer on top of the graphene was etched away without permitting the liquid to enter the capillary by placing the sample upside down over the acetone bath. In addition to providing a high yield rate, this new technique enabled the fabrication of freestanding graphene membranes with very large dimensions of up to a half-millimeter in diameter for a circular hole, as shown in Figure 5. This is the largest freestanding monatomic graphene membrane ever reported. In Figure 5a, freestanding graphene on a square hole with an edge of 300 μm (its diagonal length is roughly 424 μm) was also demonstrated to show that the IFM is an effective method to fabricate freestanding graphene membranes with sharp corners. The size and success rate of freestanding membrane can be dependent on the shape of the gap, as described in Figure S6.

Characterization of Freestanding CVD Graphene with Large Dimension. Freestanding graphene membranes may be utilized in a variety of applications, and a combination of optical microscopy and the large freestanding graphene structures offers a useful approach to the easy and rapid inspection of CVD graphene. As shown in Figure 5a, optical microscopy can discern a variety of geometric features in CVD graphene, including wrinkles, multilayer islands, and PMMA residue, while electron microscopy images of them shown in Figure S7 often suffer from a low contrast and damages by electron beam.

Figure 5b and Table S3 show the Raman spectra of various geometric features in freestanding CVD graphene. These features correspond to the red circles in the optical microscopy image in Figure 5a. The Raman spectrum measured in the monolayer region of the

freestanding graphene membrane showed a negligible D peak, indicating that this region was composed of high-quality CVD graphene. A comparison to the Raman spectrum of CVD graphene prepared on a substrate revealed that the IFM membrane spectrum was shifted slightly to the left and the 2D and G peak intensity ratio was higher. These results were attributed to the absence of substrate effects[30] and the residual tensile strain imposed on the freestanding graphene.[31,32] In addition, many wrinkles in the graphene were readily distinguished by optical microscopy, as well. The wrinkles mainly formed by mechanical folding during the transfer process as a result of the thermal expansion mismatch between the graphene and the metal catalyst (Cu).[33] The wrinkles on the graphene structure were found to be a three-layer graphene structure,[15] as confirmed by the heights of the wrinkles determined by AFM topography in Figure 5c. The Raman spectrum of the wrinkles exhibited an increase in the G and 2D peak intensities with only a small change in the ratio of the intensities. These results indicated that the Raman spectrum more closely resembled the spectrum obtained from monolayer graphene than from bilayer or trilayer graphene. This property of the wrinkle was attributed to misorientation among the stacked graphene layers.[18,34] Furthermore, Figure 5a shows the presence of many multilayer islands in the CVD graphene. The multilayer islands mainly arose from the thicker graphene regions nucleated at impurities in the Cu foil used in the synthesis process.[35] The spectra measured inside the islands corresponded to bilayer, trilayer, or even thicker graphene.[36] Tiny amounts of PMMA residue remained on the graphene membranes after the IFM process, but the quantity of the residue is no more than that on the membranes prepared by the conventional dipping method. Figure S7c shows the Raman mapping result on the whole area of freestanding CVD graphene membrane, indicating that the CVD graphene used in this report consists of mostly monolayer graphene, and the wrinkles and multilayer islands are uniformly distributed over monolayer regions. Transmission electron microscopy images (not included here) show that our CVD graphene is mainly monolayer with some multilayer islands and many wrinkles, and its grain size ranges from 5 to 10 μm.

CONCLUSION

In conclusion, the mechanism by which the freestanding CVD graphene rupture was visualized during the etchant drying process using high-speed photography and WLI techniques. The driving force responsible for the rupture was the capillary pressure and the formation of a triple junction arc. The role of the triple junction arc was very significant compared to the capillary pressure. On the basis of our understanding of the rupture mechanism, we devised the IFM technique for fabricating freestanding membranes and demonstrated that the resulting CVD graphene membranes of monatomic layer could bridge gaps up to a half-millimeter scale. The very large diameter freestanding graphene membranes would be utilized for easy and rapid inspection on the quality of synthesized CVD graphene. A variety of features, including wrinkles, pinholes, and multilayer islands on freestanding CVD graphene were clearly observable using optical microscopy. The proposed IFM technique provides a powerful route for understanding the mechanics of the CVD graphene and for preparing freestanding CVD graphene with high yield and large dimension for use in many applications. Furthermore, the proposed method can be readily extended to other two-dimensional nanomaterials, such as BN and MoS_2, for fabricating additional freestanding structures, which will enable another device fabrication and property characterization for the variety of applications.

METHODS

Synthesis of the Graphene by CVD and the Subsequent Transfer. Graphene was grown on a copper foil using chemical vapor deposition. The copper foil (99.8% purity and 25 μm thickness, no. 13382, Alfa Aesar) was loaded into a tubular quartz tube and heated to 1000 °C under the flow of 8 sccm H_2 at 90 mTorr. After reaching 1000 °C, the foil was annealed for 30 min without changing the flow rate or pressure. A gas mixture comprising CH_4 and H_2 was then introduced at 460 mTorr at rates of 24 and 8 sccm, respectively, for 30 min. Finally, the foil was cooled to room temperature under the flow of H_2 at a pressure of 90 mTorr. PMMA (A4, Microchem 950, 4000 rpm for 30 s) was spin-coated onto the graphene/copper foils and thermally cured on a hot plate heated to 80 °C for 60 s. The copper foil was etched with ammonium persulfate solution (Sigma-Aldrich, $(NH_4)_2S_2O_8$, 12.5 g/L), and the PMMA/graphene was rinsed in a distilled water reservoir for 1 day. Perforated SiO_2/Si substrates (500 μm thick with a 300 nm SiO_2 layer) were treated with O_2 plasma to create hydrophilic SiO_2/Si substrate surfaces. PMMA/graphene was transferred onto the perforated SiO_2/Si substrates. The graphene on SiO_2/Si substrates was then heated in an oven (80 °C, 1 h) to improve the adhesion between the substrate and the graphene.

Inverted Floating Method. The PMMA layer was removed by exposing the PMMA layer only to acetone. The removal of the PMMA was ensured by tilting the sample slightly using a jig with variable spacers. The dissolution step was performed over a period of 3 h. The temperature of the acetone was kept at 50 °C during the process to promote the dissolution. After removing the PMMA, the sample was quickly raised to a vertical position to avoid leaving any residues on the graphene surface. The sample was not annealed at high temperatures. Under high-temperature conditions, freestanding CVD graphene membranes can be easily broken by thermal expansion mismatch between the graphene and the substrate.

Characterization. A 514 nm excitation laser was directed through a 100× objective lens (inVia Raman microscope, Renishaw) to the sample, and a 1800 line/mm grating was used to obtain the Raman spectra. The laser spot size was about 1 μm in diameter. The AFM measurements shown in Figure S7a were

performed on a graphene sample transferred onto a flat SiO_2 substrate. The contact mode was used with a set point of 0.2 nN and a scanning rate of 0.1 Hz (NanoWizard, JPK Instruments). Prior to conducting the AFM measurements, thermal annealing was applied to the graphene sample under an Ar flow of 500 sccm at 350 °C under low vacuum conditions to remove any residual PMMA and to improve adhesion between the graphene and the SiO_2 substrate.

High-Speed Imaging and White Light Interferometry. High-speed photography was conducted using a Fastcam 1024 PCI (Photron USA, Inc.) system at a frame rate of 3000 frames/s and an image resolution of 512 × 512 pixels. As shown in the Supporting Information movie S1, the liquid drying process and the formation and growth of the triple junction arc could be clearly visualized. WLI was performed using a NewView 6300 system (Zygo Co.) and a Mirau-type interferometric objective lens with a low-reflectance reference mirror (Zygo Co.). Enhanced fringe contrast was obtained from the graphene, which had a low reflectance. The deformation of the graphene membrane during the drying process was quantitatively measured by WLI at a frame rate of 1 frame/s. This information helped us to understand the mechanics of the drying process.

Conflict of Interest: The authors declare no competing financial interest.

Acknowledgment. We thank Mr. Don Battistoni at Zygo for the white light interferometry measurements. We also thank Dr. Dae-Geun Choi at KIMM for providing the $C_4F_9OCH_3$ liquid. This research was supported by the Industrial Core Technology Development Programs of the Korean Ministry of Knowledge Economy (Grant 10033309), the National Platform Technology Programs of the Korean Ministry of Knowledge Economy (Grant 10034751), and the Basic Science Research Program through the National Research Foundation of Korea (NRF) funded by the Ministry of Education, Science and Technology (2011-0010156).

Supporting Information Available: Additional procedures for freestanding graphene membranes, contact angles of graphene/SiO_2 and SiO_2 substrates, details of rupture mechanics in a freestanding CVD graphene during the drying process, role of microscopic defects in the rupture of freestanding CVD graphene, and characterization of the CVD graphene membranes. This material is available free of charge *via* the Internet at http://pubs.acs.org.

REFERENCES AND NOTES

1. Zhang, Y.; Brar, V. W.; Girit, C.; Zettl, A.; Crommie, M. F. Origin of Spatial Charge Inhomogeneity in Graphene. *Nat. Phys.* **2009**, *5*, 722–726.
2. Bolotin, K. I.; Sikes, K. J.; Jiang, Z.; Klima, M.; Fudenberg, G.; Hone, J.; Kim, P.; Stormer, H. L. Ultrahigh Electron Mobility in Suspended Graphene. *Solid State Commun.* **2008**, *146*, 351–355.
3. Sorkin, V.; Zhang, Y. W. Graphene-Based Pressure Nano-Sensors. *J. Mol. Model.* **2011**, *17*, 2825–2830.
4. Bunch, J. S.; Verbridge, S. S.; Alden, J. S.; van der Zande, A. M.; Parpia, J. M.; Craighead, H. G.; McEuen, P. L. Impermeable Atomic Membranes from Graphene Sheets. *Nano Lett.* **2008**, *8*, 2458–2462.
5. Gautam, M.; Jayatissa, A. H. Gas Sensing Properties of Graphene Synthesized by Chemical Vapor Deposition. *Mater. Sci. Eng., C* **2011**, *31*, 1405–1411.
6. Schedin, F.; Geim, A. K.; Morozov, S. V.; Hill, E. W.; Blake, P.; Katsnelson, M. I.; Novoselov, K. S. Detection of Individual Gas Molecules Adsorbed on Graphene. *Nat. Mater.* **2007**, *6*, 652–655.
7. Ren, Y.; Zhu, C.; Cai, W.; Li, H.; Ji, H.; Kholmanov, I.; Wu, Y.; Piner, R. D.; Ruoff, R. S. Detection of Sulfur Dioxide Gas with Graphene Field Effect Transistor. *Appl. Phys. Lett.* **2012**, *100*, 163114.
8. Park, J. J.; Lee, K. J. B.; Wright, O. B.; Jung, M. K.; Lee, S. H. Giant Acoustic Concentration by Extraordinary Transmission in Zero-Mass Metamaterials. *Phys. Rev. Lett.* **2013**, *110*, 244302.
9. Bunch, J. S.; van der Zande, A. M.; Verbridge, S. S.; Frank, I. W.; Tanenbaum, D. M.; Alden, J. S.; Parpia, J. M.; Craighead, H. G.; McEuen, P. L. Electromechanical Resonators from Graphene Sheets. *Science* **2007**, *315*, 490–493.
10. van der Zande, A. M.; Barton, R. A.; Alden, J. S.; Ruiz-Vargas, C. S.; Whitney, W. S.; Pham, P. H. Q.; Park, J.; Parpia, J. M.; Craighead, H. G.; McEuen, P. L. Large-Scale Arrays of Single-Layer Graphene Resonators. *Nano Lett.* **2010**, *10*, 4869–4873.
11. Song, X.; Oksanen, M.; Sillanpää, M. A.; Craighead, H. G.; Parpia, J. M.; Hakonen, P. J. Stamp Transferred Suspended Graphene Mechanical Resonators for Radio Frequency Electrical Readout. *Nano Lett.* **2012**, *12*, 198–202.
12. Booth, T. J.; Blake, P.; Nair, R. R.; Jiang, D.; Hill, E. W.; Bangert, U.; Bleloch, A.; Gass, M.; Novoselov, K. S.; Katsnelson, M. I.; *et al.* Macroscopic Graphene Membranes and Their Extraordinary Stiffness. *Nano Lett.* **2008**, *8*, 2442–2446.
13. Alemán, B.; Regan, W.; Aloni, S.; Altoe, V.; Alem, N.; Girit, C.; Geng, B.; Maserati, L.; Crommie, M.; Wang, F.; *et al.* Transfer-Free Batch Fabrication of Large-Area Suspended Graphene Membranes. *ACS Nano* **2010**, *4*, 4762–4768.
14. Suk, J. W.; Kitt, A.; Magnuson, C. W.; Hao, Y.; Ahmed, S.; An, J.; Swan, A. K.; Goldberg, B. B.; Ruoff, R. S. Transfer of CVD-Grown Monolayer Graphene onto Arbitrary Substrates. *ACS Nano* **2011**, *5*, 6916–6924.
15. Kim, K.; Lee, Z.; Regan, W.; Kisielowski, C.; Crommie, M. F.; Zettl, A. Grain Boundary Mapping in Polycrystalline Graphene. *ACS Nano* **2011**, *5*, 2142–2146.
16. Huang, P. Y.; Ruiz-Vargas, C. S.; van der Zande, A. M.; Whitney, W. S.; Levendorf, M. P.; Kevek, J. W.; Garg, S.; Alden, J. S.; Hustedt, C. J.; Zhu, J.; *et al.* Grains and Grain Boundaries in Single-Layer Graphene Atomic Patchwork Quilts. *Nature* **2011**, *469*, 389–392.
17. Ruiz-Vargas, C. S.; Zhuang, H. L.; Huang, P. Y.; van der Zande, A. M.; Garg, S.; McEuen, P. L.; Muller, D. A.; Hennig, R. G.; Park, J. Softened Elastic Response and Unzipping in Chemical Vapor Deposition Graphene Membranes. *Nano Lett.* **2011**, *11*, 2259–2263.
18. Bae, S.; Kim, H.; Lee, Y.; Xu, X.; Park, J. S.; Zheng, Y.; Balakrishnan, J.; Lei, T.; Kim, H. R.; Song, Y. I.; *et al.* Roll-to-Roll Production of 30-Inch Graphene Films for Transparent Electrodes. *Nat. Nanotechnol.* **2010**, *5*, 574–578.
19. Liang, X.; Sperling, B. A.; Calizo, I.; Cheng, G.; Hacker, C. A.; Zhang, Q.; Obeng, Y.; Yan, K.; Peng, H.; Li, Q.; *et al.* Toward Clean and Crackless Transfer of Graphene. *ACS Nano* **2011**, *5*, 9144–9153.
20. Regan, W.; Alem, N.; Alemán, B.; Geng, B.; Girit, C.; Maserati, L.; Wang, F.; Crommie, M.; Zettl, A. A Direct Transfer of Layer-Area Graphene. *Appl. Phys. Lett.* **2010**, *96*, 113102.
21. Lin, Y.-C.; Jin, C.; Lee, J.-C.; Jen, S.-F.; Suenaga, K.; Chiu, P.-W. Clean Transfer of Graphene for Isolation and Suspension. *ACS Nano* **2011**, *5*, 2362–2368.
22. Zabel, J.; Nair, R. R.; Ott, A.; Georgiou, T.; Geim, A. K.; Novoselov, K. S.; Casiraghi, C. Raman Spectroscopy of Graphene and Bilayer under Biaxial Strain: Bubbles and Balloons. *Nano Lett.* **2012**, *12*, 617–621.
23. Jasper, J. J. The Surface Tension of Pure Liquid Compounds. *J. Phys. Chem. Ref. Data* **1972**, *1*, 841–1009.
24. Tuğrul, A. B. Capillarity Effect Analysis for Alternative Liquid Penetrant Chemicals. *NDT&E Int.* **1997**, *30*, 19–23.
25. Lee, C.; Wei, X.; Kysar, J. W.; Hone, J. Measurement of the Elastic Properties and Intrinsic Strength of Monolayer Graphene. *Science* **2008**, *321*, 385–388.
26. Lee, G.-H.; Cooper, R. C.; An, S. J.; Lee, S.; van der Zande, A.; Petrone, N.; Hammerberg, A. G.; Lee, C.; Crawford, B.; Oliver, W.; *et al.* High-Strength Chemical-Vapor-Deposited Graphene and Grain Boundaries. *Science* **2013**, *340*, 1073–1076.
27. Lin, Q. Y.; Jing, G.; Zhou, Y. B.; Wang, Y. F.; Meng, J.; Bie, Y. Q.; Yu, D. P.; Liao, Z. M. Stretch Induced Stiffness Enhancement of CVD Graphene. *ACS Nano* **2013**, *7*, 1171–1177.
28. Grantab, R.; Shenoy, V. B.; Ruoff, R. S. Anomalous Strength Characteristics of Tilt Grain Boundaries in Graphene. *Science* **2010**, *330*, 946–948.

29. Tsen, A. W.; Brown, L.; Levendorf, M. P.; Ghahari, F.; Huang, P. Y.; Havener, R. W.; Ruiz-Vargas, C. S.; Muller, D. A.; Kim, P.; Park, J. Tailoring Electrical Transport across Grain Boundaries in Polycrystalline Graphene. *Science* **2012**, *336*, 1143–1146.
30. Berciaud, S.; Ryu, S.; Brus, L. E.; Heinz, T. F. Probing the Intrinsic Properties of Exfoliated Graphene: Raman Spectroscopy of Free-Standing Monolayers. *Nano Lett.* **2009**, *9*, 346–352.
31. Tang, B.; Guoxin, H.; Gao, H. Raman Spectroscopic Characterization of Graphene. *Appl. Spectrosc. Rev.* **2010**, *45*, 369–407.
32. Huang, M.; Yan, H.; Chen, C.; Song, D.; Heinz, T. F.; Hone, J. Phonon Softening and Crystallographic Orientation of Strained Graphene Studied by Raman Spectroscopy. *Proc. Natl. Acad. Sci. U.S.A.* **2009**, *106*, 7304–7308.
33. Zhu, W.; Low, T.; Perebeinos, V.; Bol, A. A.; Zhu, Y.; Yan, H.; Tersoff, J.; Avouris, P. Structure and Electronic Transport in Graphene Wrinkles. *Nano Lett.* **2012**, *12*, 3431–3436.
34. Yan, K.; Peng, H.; Zhou, Y.; Li, H.; Liu, Z. Formation of Bilayer Bernal Graphene: Layer-by-Layer Epitaxy *via* Chemical Vapor Deposition. *Nano Lett.* **2011**, *11*, 1106–1110.
35. Wang, H.; Wang, G.; Bao, P.; Yang, S.; Zhu, W.; Xie, X.; Zhang, W. Controllable Synthesis of Submillimeter Single-Crystal Monolayer Graphene Domains on Copper Foils by Suppressing Nucleation. *J. Am. Chem. Soc.* **2012**, *134*, 3627–3630.
36. Malarda, L. M.; Pimenta, M. A.; Dresselhaus, G.; Dresselhaus, M. S. Raman Spectroscopy in Graphene. *Phys. Rep.* **2009**, *473*, 51–87.